Theory of oxygen tracer diffusion along grain boundaries and in the bulk in two-stage oxidation experiments. Part I: formulation of the model and analysis of type A and C regimes

Yu. Mishin, G. Borchardt

Classification
Physics Abstracts
66.30 — 81.60B

Theory of oxygen tracer diffusion along grain boundaries and in the bulk in two-stage oxidation experiments. Part I : formulation of the model and analysis of type A and C regimes

Yu. M. Mishin (*) and G. Borchardt

Sonderforschungsbereich 180 and Institut für Allgemeine Metallurgie, Technische Universität Clausthal, Robert-Koch-Strasse 42, D-3392 Clausthal-Zellerfeld, Germany

(*Received 17 July 1992, revised 11 December 1992, accepted 14 December 1992*)

Résumé. — Pour un modèle simple de croissance de couche d'oxyde et pour une expérience d'oxydation à deux étapes, la deuxième étape est décrite par les équations de diffusion d'un traceur d'oxygène. A l'aide de ce formalisme, nous analysons des profils de traceurs en fonction de la température, du temps et du mécanisme de transport. Dans la partie I, nous considérons le régime A à haute température et le régime C à basse température. Les résultats sont présentés sous forme de diagrammes cinétiques qui permettent d'interpréter les expériences. La partie II sera consacrée au régime intermédiaire B.

Abstract. — Based on a simple model of oxide film growth, we derive equations for oxygen tracer diffusion during the second stage in two-stage oxidation experiments. Using this model, we analyze tracer penetration profiles depending on temperature, time and the atomic mechanism of oxygen transport. In Part I the high-temperature A and the low-temperature C regimes of diffusion are considered. The results are presented as kinetic diagrams convenient for designing and interpreting experiments. Part II of this work will be devoted to the intermediate regime B.

1. Introduction.

An effective approach to the studies of thermal oxide film growth consists in conducting two-stage oxidation experiments using the stable oxygen isotope ^{18}O (see e.g. recent reviews [1-3]). In such experiments, the substrate is first oxidized in an oxygen-bearing atmosphere with the natural isotope composition ($\simeq 99.76\,\%\ ^{16}O$) and then in an atmosphere enriched in ^{18}O. Having measured by SIMS, RBS or nuclear reaction techniques the isotope distribution profile in the sample, one can extract valuable information concerning transport mechanisms that control the oxide film growth. This approach implies the comparison of the obtained experimental profiles with those predicted theoretically for various situations depending on the

(*) *Permanent address :* Russian Institute of Aviation Materials, 17 Radio Street, 107005 Moscow, Russia.

nature of the diffusing species (oxygen or metal), prevailing diffusion paths (lattice or short circuits), and other factors.

The present paper deals with the second, theoretical side of the problem. The purpose will be to carry out a detailed analysis of possible tracer profiles in conditions when they are determined by grain boundary (GB) diffusion in the film. Based on a simple model, we identify possible kinetic regimes of self-diffusion of oxygen tracer in a growing oxide film and present analytical solutions for tracer penetration profiles corresponding to each of the regimes. Special attention is paid to problems of experimental profiles treatment and two-stage experiments designing.

GB diffusion is commonly admitted to play a crucial role in oxide film growth. This circumstance was taken into account in the basic work by Basu and Halloran [4], who were the first to predict qualitatively different oxygen tracer profiles depending on the transport mechanism of oxide growth. As far as the quantitative side is concerned, both in Basu and Halloran's work [4] and in a more recent study [5] GB diffusion was treated in terms of the spherical grain model, previously proposed by Oishi and Ichimura [6] for diffusion in oxides and still earlier by Bokshtein *et al.* [7] for diffusion in metals. In contrast, the present analysis is based on the parallel GBs model (Fig. 1), which has the following advantages :

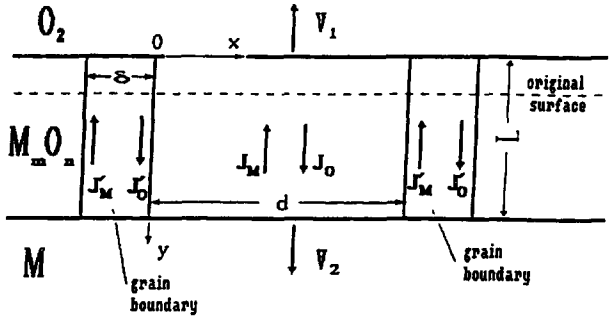

Fig. 1. — Schematic geometry in the present model of oxide film growth.

First, the parallel GBs model is capable of describing the whole spectrum of possible diffusion regimes in a polycrystalline material : A, B and C in Harrison's classification [8] (see [9] for more detail). At the same time the spherical grain model, giving for the B and C-regimes practically the same penetration profiles as the model of parallel GBs, fails to give the correct picture of diffusion in the A-regime. The spherical symmetry of this model excludes any long-range mass transport by lattice diffusion, as a result of which the effective diffusivity of the polycrystalline material, D_{eff}, appears to coincide with the GB diffusivity D' [7, 9]. The latter relation is clearly erroneous since, in general, both GB and lattice diffusion contribute to D_{eff} more or less in accordance with the Hart formula [10]

$$D_{\text{eff}} \simeq \nu D' + (1 - \nu) D \,. \tag{1}$$

(D is the lattice diffusion coefficient, ν the atomic fraction of GB sites in the polycrystal). Even for a fine-grained material, when the first term in equation (1) prevails over the second one, we still have $D_{\text{eff}} \simeq \nu D' \ll D'$ since normally $\nu \ll 1$.

Second, the theory of diffusion along an array of parallel GBs or a single planar GB has been developed to a much better degree (see e.g. reviews [9, 11, 12]) compared to the spherical grain model, at least on the mathematical side. Hence it seems advantageous to draw the

results, available in that field, for the purposes of the present work. Furthermore, there is a close similarity between GB diffusion in a growing oxide film and GB-electromigration in a thin metal film. While dealing with the parallel GBs model one can make use of some interesting theoretical results and ideas developed for GB electromigration in the same model [11, 13-16].

Lastly, in reality the outer layer of a growing oxide film may often exhibit a columnar grain structure, as is the case e.g. for NiO [17], CoO [18], and Fe_3O_4 [19]. In such cases the model of parallel GBs seems to be more relevant than the spherical model.

This work consists of two parts : in part I we introduce a simple growth model of a columnar-grained oxide film and derive basic equations for ^{18}O diffusion at the second stage of a « double oxidation » experiment. Together with the corresponding boundary conditions, these equations represent a mathematical formulation of the model, appropriate for numerical simulation of the tracer penetration profiles. We carry out a detailed kinetic analysis of the most important extreme cases of the theory. For each of the cases an analytical solution of the model is presented and the expected shape of the oxygen tracer profile is evaluated. Part I deals with type A and type C kinetic regimes which prevail at relatively high and relatively low temperatures, respectively. Part II will be entirely devoted to the intermediate, type B regime which is the most difficult case to analyze. We shall derive a new analytical solution of the model which is essentially more general than the previous solutions and applies to both B and C type regimes as special cases.

2. The model of oxide film growth.

Suppose we have a continuous oxide film bounded by two parallel plane interfaces : oxide/atmosphere and oxide/substrate (Fig. 1). The oxide nucleation and earlier stages of its growth will not be considered. Rather, the attention will be focused on later stages of the oxidation reaction when diffusion controlled thickening of the film occurs. The thickening kinetics at this step will be treated in terms of Wagner's theory [20] which suggests that diffusion of the species across the film is the rate-controlling step of the oxidation process. To be more specific, we shall consider the growth of an oxide M_mO_n on a metal substrate (M) with vanishing oxygen solubility. In fact, however, our analysis can be extended to oxidation of metallic alloys, ceramic materials, as well as to other solid-gas reactions in which the product binary compound (such as sulfide, chloride, or nitride) is growing as a continuous planar layer on the surface.

Neglecting, at first, GB diffusion effects, we can estimate the velocities of the interfaces oxide/gas (V_1) and oxide/metal (V_2) as

$$V_1 = J_M/c_M \quad \text{and} \quad V_2 = J_O/c_O \,. \tag{2}$$

Here c_O and c_M are concentrations (in cm^{-3}) of oxygen and metal, respectively. J_O and J_M are the corresponding fluxes (in $cm^{-2}\,s^{-1}$) which, under quasi-steady conditions, are assumed to be coordinate-independent (note that $J_M < 0$). It is also adopted that the oxidation reaction occurs only at the interfaces : generally, both at the oxide/gas interface to the measure of cations supply (flux J_M) and at the oxide/metal interface to the measure of anions supply (flux J_O). Importantly, we are fixed to the reference system of the oxide lattice in which the metal lattice experiences, in general, some motion as a whole. In this (and only in this) system of reference the fluxes J_O and J_M can be related to the respective self-diffusion coefficients, D_O and D_M, *via* the standard chemical diffusion equations [20] :

$$J_O = -\frac{c_O}{kTL}\int_{\mu_0}^{\mu_L} D_O \, d\mu, \quad J_M = \frac{c_O}{kTL}\int_{\mu_0}^{\mu_L} D_M \, d\mu \,, \tag{3}$$

where k is Boltzmann's constant, T temperature, L an instantaneous thickness of the film. Both of the equations (3) are expressed in terms of oxygen chemical potential μ since the metal chemical potential μ_M is related to μ *via* the Gibbs-Duhem equation $c_O\,d\mu + c_M\,d\mu_M = 0$. The boundary values of μ at $y = 0$ and $y = L$ are denoted as μ_0 and μ_L, respectively. According to relations (2) and (3), the total growth velocity $V_2 - V_1$ is inversely proportional to L, which leads to the parabolic growth law $L^2 = 2\,Kt$ with the rate constant

$$K = \frac{1}{kT}\int_{\mu_L}^{\mu_0}\left(D_O + \frac{n}{m}D_M\right)\,d\mu\,. \tag{4}$$

Now let us consider a polycrystalline film in which the GBs are parallel to each other and normal to the interphase boundaries (see Fig. 1). Suppose, during the film growth the GBs keep in thermodynamic equilibrium with the lattice, which means that μ has the same value both in the GBs and in the bulk (lattice) at any given depth y. Then, the bulk diffusion fluxes are again determined by equations (3), whereas the GB diffusion fluxes, J'_O and J'_M, are determined by the relations

$$J'_O = -\frac{c_O}{kTL}\int_{\mu_0}^{\mu_L} D'_O\,d\mu, \quad J'_M = \frac{c_O}{kTL}\int_{\mu_0}^{\mu_L} D'_M\,d\mu\,, \tag{5}$$

where D'_O and D'_M are the GB self-diffusion coefficients of the species. Since normally $D'_O \gg D_O$ and $D'_M \gg D_M$, the GB fluxes are much greater than the respective bulk fluxes, and therefore the GB growth velocities, $V'_1 = J'_M/c_M$ and $V'_2 = J'_O/c_O$, should be considerably greater than the bulk velocities (2). This, in turn, might result in the stresses generation near the GB/interphase lines, as well as in the roughening of the outer surface of the film and in the growth of pegs and protrusions at the oxide/metal interface. However, we shall introduce the simplifying assumption that both of the interfaces remain plane during the film growth. For instance, this can be the case when diffusion of the species along the interfaces proceeds much faster than GB diffusion, thereby self-maintaining the planar geometry of the film.

Under the above assumption the metal (oxygen) atoms supplied by both the GB and bulk diffusion are uniformly redistributed over the moving oxide/gas (oxide/metal) interface. According to the material balance, the corresponding growth velocities are given by

$$V_1 = [\nu J'_M + (1-\nu)J_M]/c_M\,, \quad V_2 = [\nu J'_O + (1-\nu)J_O]/c_O\,. \tag{6}$$

The GB fraction $\nu = \delta/(d+\delta)$ depends on the GB width δ and the distance, d, between the GBs. Again we arrive at the parabolic kinetics law, but now the rate constant

$$K = \frac{1}{kT}\int_{\mu_L}^{\mu_0} D_{eff}\,d\mu \tag{7}$$

is determined by the effective diffusion coefficient

$$D_{eff} = \nu\left(D'_O + \frac{n}{m}D'_M\right) + (1-\nu)\left(D_O + \frac{n}{m}D_M\right)\,. \tag{8}$$

This simple model of oxide film growth forms the basis for the further analysis.

3. Tracer diffusion equations.

Now let us consider the second stage of the experiment, when starting from a certain moment $t = 0$ oxidation is continued at the same temperature and at the same oxygen partial pressure

but with a higher ratio $^{18}O/^{16}O$ compared to that in the natural atmosphere. The aim is to derive equations for the ^{18}O tracer transport in the film in the course of its further growth.

This may be done in terms of the excess tracer concentration (fraction), c, determined by

$$c \equiv \frac{c_{18}}{c_{18} + c_{16}} - \left(\frac{c_{18}}{c_{18} + c_{16}} \right)_{\text{nat.}}, \tag{9}$$

where the last term refers to the natural abundance of ^{18}O ($\simeq 0.25$ %). Then, the excess tracer flux $\mathbf{J}_O^*$ in the bulk is given by

$$\mathbf{J}_O^* = c\mathbf{J}_O - D_O^* c_O \nabla c . \tag{10}$$

Here D_O^* is the tracer self-diffusion coefficient, related with the self-diffusion coefficient D_O by $D_O^* = fD_O$, f being the correlation factor for self-diffusion. To be shorter, hereinbelow D_O^* is designated as simply D. Combined with the continuity equation

$$\frac{\partial (cc_O)}{\partial t} + \operatorname{div} \mathbf{J}_O^* = 0 ,$$

equation (10) gives the tracer diffusion equation

$$\frac{\partial c}{\partial t} = \nabla (D \nabla c) - \frac{J_O}{c_O} \frac{\partial c}{\partial y} \tag{11}$$

In the same manner, the GB tracer diffusion follows the equation

$$\frac{\partial c'}{\partial t} = \nabla (D' \nabla c) - \frac{J'_O}{c_O} \frac{\partial c'}{\partial y}, \tag{12}$$

in which c' is the excess tracer concentration in the GBs and $D' \equiv D_O^{*\prime} = f' D'_O$ is the coefficient of GB self-diffusion of ^{18}O.

Up to here we were fixed to the reference frame of the oxide lattice. However, we are more interested in diffusion in the frame of reference fixed to the oxide/gas interface since in experiments the isotope profiles are measured relative to the specimen surface. In the new frame of reference the oxide lattice is generally moving along the y axis with the velocity $-V_l$. Therefore, a term $-\mathbf{V}_l cc_O$ should be added to the right-hand sides of equation (10) and of the corresponding flux equation for the GBs. As a result equations (11) and (12) take the form

$$\frac{\partial c}{\partial t} = \nabla (D \nabla c) - V \frac{\partial c}{\partial y} \qquad \text{(bulk diffusion)}, \tag{13}$$

$$\frac{\partial c'}{\partial t} = \nabla (D' \nabla c) - V' \frac{\partial c'}{\partial y} \qquad \text{(GB diffusion)}, \tag{14}$$

where the coefficients

$$V \equiv J_O/c_O - V_l = \frac{1}{kTL} \int_{\mu_L}^{\mu_0} \left\{ D_O + \frac{n}{m} [\nu D'_M + (1 - \nu) D_M] \right\} d\mu \tag{15}$$

and

$$V' \equiv J'_O/c_O - V_l = \frac{1}{kTL} \int_{\mu_L}^{\mu_0} \left\{ D'_O + \frac{n}{m} [\nu D'_M + (1 - \nu) D_M] \right\} d\mu \tag{16}$$

have the meaning of drift velocities of the oxygen tracer in the bulk and in the GBs, respectively. In the same way as it is done in the Fisher model [9, 21, 22], the GB diffusion equation (14) can be approximated by

$$\frac{\partial c'}{\partial t} = \frac{\partial}{\partial y}\left(D'\frac{\partial c'}{\partial y}\right) + \frac{2D}{\delta}\left(\frac{\partial c}{\partial x}\right)_{x=0} - V'\frac{\partial c'}{\partial y}, \tag{17}$$

where the second term in the right-hand side takes into account the loss (or gain) of the tracer from (or by) the GBs.

Thus, tracer diffusion in a growing film can be described by two coupled equations, (13) and (17), for two concentration functions, $c(x, y, t)$ and $c'(y, t)$. Due to the symmetry, these equations should be solved in the rectangular area, $0 \leq x \leq d/2$ and $0 \leq y \leq L$, with the following boundary conditions :

$$c(x, y, 0) = c'(y, 0) = 0\,; \quad \text{(initial condition)} \tag{18}$$

$$c(x, 0, t) = c'(0, t) = c_0\,; \quad \text{(constant source)} \tag{19}$$

$$c(x, L, t) = c'(L, t)\,; \quad \text{(fast interphase diffusion)} \tag{20}$$

$$c(0, y, t) = c'(y, t)\,; \quad \text{(GB/bulk joining condition)} \tag{21}$$

$$(\partial c/\partial x)_{x=d/2} = 0\,; \quad \text{(symmetry)} \tag{22}$$

$$[\nu D'(\partial c'/\partial y) + (1-\nu)D(\partial c/\partial y)]_{y=L} = 0\,. \quad \text{(zero tracer flux)} \tag{23}$$

Conditions (18) and (19) suggest that at the moment $t = 0$ the excess concentration of ^{18}O instantaneously increases at the surface from zero to c_0 and remains at this level during the subsequent annealing. If and when the isotope ^{18}O penetrating into the growing film reaches the oxide/metal interface, its interfacial concentration is assumed to be dependent only on time but not on x. Indeed, as was mentioned above, fast diffusion along the oxide/metal interface admittedly ensures nearly uniform distribution of oxygen, including ^{18}O, over the interface.

The oxide/metal interface moves according to the parabolic law

$$L(t) = [2K(t + t_0)]^{1/2}, \tag{24}$$

where t_0 denotes the duration of the first, tracer-free stage of the experiment. Accordingly, the instantaneous velocity of the interface, V_L, equals

$$V_L = V_2 - V_1 = (K/2)^{1/2}\,(t + t_0)^{-1/2} \tag{25}$$

Note that, as it follows from relations (6),

$$V_L = \nu V' + (1-\nu)V\,, \tag{26}$$

and thereby the drift velocities (15) and (16) always satisfy the inequality

$$V \leq V_L \leq V' \tag{27}$$

To derive the boundary condition (23), note that at $y = L$ both the tracer and the total oxygen fluxes, considered relative to the surface, must satisfy the mass balance relations

$$\nu J_O^{*\prime} + (1-\nu)J_O^{*} = cc_O V_L \quad \text{and} \quad \nu J_O' + (1-\nu)J_O = c_O V_L\,. \tag{28}$$

At the same time, using equations (10) and (20) and taking into account that at $y = L$ the fluxes are normal to the interface, we have

$$J_O^{*} = cJ_O - Dc_O\frac{\partial c}{\partial y} \quad \text{and} \quad J_O^{*\prime} = cJ_O' - D'c_O\frac{\partial c'}{\partial y} \tag{29}$$

Combining equations (28) and (29), one obtains condition (23).

A major problem associated with equations (13) and (17) consists in a very strong coordinate dependence of the tracer diffusion coefficients, which arises from specific atomic mechanisms of chemical diffusion in oxides. The ionic transport is provided by maintaining a great difference in defect (vacancy or interstitial) concentration between the oxide/gas and oxide/metal interfaces. Since the self-diffusion coefficient is roughly proportional to the defect concentration, it also greatly changes across the film. In principle, this circumstance should be taken into account in equations (13) and (17), especially when the tracer penetration length is comparable with the film thickness. In this paper, however, we shall restrict ourselves to considering a simplified version of the model in which the diffusivities D and D' are fixed at constant values, namely, at their true values near the surface ($y = 0$). Strictly, this approximation can only work when

$$\left(\frac{\partial \ln D}{\partial y} \right) \ell \ll 1 \quad \text{and} \quad \left(\frac{\partial \ln D'}{\partial y} \right) \ell' \ll 1 , \tag{30}$$

ℓ' and ℓ being tracer penetration lengths along the GBs and in the bulk, respectively. However, we shall also have to consider situations when one or both of the lengths are comparable with L, in which cases conditions (30) no longer hold. We can hope, nevertheless, that even in such cases the model may give qualitatively correct results.

Taking into account the above assumption, equations (13) and (17) become

$$\frac{\partial c'}{\partial t} = D' \frac{\partial^2 c'}{\partial y^2} + \frac{2D}{\delta} \left(\frac{\partial c}{\partial x} \right)_{x=0} - V' \frac{\partial c'}{\partial y} , \tag{31}$$

$$\frac{\partial c}{\partial t} = D \left(\frac{\partial^2 c}{\partial x^2} + \frac{\partial^2 c}{\partial y^2} \right) - V \frac{\partial c}{\partial y} \tag{32}$$

Thus, we have arrived at a mathematically complete formulation of the model expressed by the differential equations (31) and (32) with the boundary conditions (18)-(23). Since the model equations depend on 11 parameters (t, t_0, x, y, D, D', V, V', K, δ and d), they can be rewritten in terms of 9 independent dimensionless variables. Having solved the equations, one can calculate the experimentally measured tracer profile $A(y, t)$, A being the layered concentration determined as

$$A(y, t) = \frac{1}{d + \delta} \left[c'(y, t)\, \delta + 2 \int_0^{d/2} c(x, y, t)\, \mathrm{d}x \right] . \tag{33}$$

Exact analytical solution of equations (31) and (32) is hardly possible and unlikely to be meaningful. In its present formulation the model is intended for computer simulation of ^{18}O profiles in two stage oxidation experiments. However, while this computer work is under way, it seems rather advantageous to carry out the analysis of various special cases when the basic equations of the model take a simplified form and their analytical solution turns out feasible. Such solutions can be very useful in numerical simulations, as it has been recently demonstrated for the spherical grain model [5]. Also, having considered a number of limiting cases one can get a good idea of the whole picture of the process, which in the present case is rather complicated. Moreover, most of real experiments either realize or, at least, can be specially designed to realize one of such limiting situations.

4. Analysis of penetration profiles in type A regime.

Let us consider the situation where $(Dt)^{1/2} \gg d$. This situation is known as A-regime [8, 9] and can be expected at relatively high temperatures, or after long anneals, or in sufficiently fine-

grained oxides. In this regime the tracer distribution is nearly uniform in the x direction and thus the bulk concentration is a function of y only. Therefore we can omit the leakage term in equation (31) and the term $\partial^2 c/\partial x^2$ in (32). Then, by adding equation (31) times ν to equation (32) times $(1 - \nu)$ and taking into account equation (26) we obtain the effective diffusion equation

$$\frac{\partial c}{\partial t} = D^*_{\text{eff}} \frac{\partial^2 c}{\partial y^2} - V_{\text{L}} \frac{\partial c}{\partial y} \tag{34}$$

Here

$$D^*_{\text{eff}} = \nu D' + (1 - \nu) D = \nu f' D'_{\text{O}} + (1 - \nu) f D_{\text{O}} \tag{35}$$

represents the effective self-diffusion coefficient of oxygen tracer. Virtually, the film behaves like a homogeneous medium with the diffusivity D^*_{eff}. Remarkably, in this case the drift velocity coincides with the internal interface velocity V_{L}.

To understand the tracer profiles behaviour predicted by equation (34) let us first consider the simplest limiting case when $D^*_{\text{eff}} \to 0$, i.e. when we have no isotope exchange. Then, equation (34) takes the form

$$\frac{\partial c}{\partial t} = - V_{\text{L}} \frac{\partial c}{\partial y} \tag{36}$$

and can be easily solved to give

$$c = c_0 H[\Delta L(t) - x] . \tag{37}$$

Here H is Heaviside's unit step function, and

$$\Delta L(t) \equiv L(t) - L(0) = [2 K(t + t_0)]^{1/2} - [2 K t_0]^{1/2} \tag{38}$$

is the total thickness of new oxide by a moment t. Solution (37) predicts a step-like profile with a sharp boundary between the zone of isotope equilibrium ($c \simeq c_0$) and the pure ^{16}O zone [1] ($c \ll c_0$) (Fig. 2a). This boundary, which we hereinafter call an isotope boundary (IB), drifts according to the law

$$y_{\text{IB}}(t) = [2 K(t + t_0)]^{1/2} - [2 K t_0]^{1/2} \tag{39}$$

The thickness of the isotope equilibrium zone equals the total thickness of the new oxide. This does not mean that this zone necessarily consists of new oxide. In a general case the new oxide grows both at the surface and at the oxide/metal interface. However, in the A-regime the tracer does not label these two new oxide layers. The tracer profile only allows one to determine the total thickness ΔL of the new oxide layers but bears no information concerning their location and relative sizes.

If D^*_{eff} is nonzero but still very small, expression (39) again holds, only that the IB is smeared to a layer of about $(D^*_{\text{eff}} t)^{1/2}$ in thickness (Fig. 2b). Lastly, if D^*_{eff} is finite whereas $V_{\text{L}} \to 0$, equation (34) reduces to the normal diffusion equation

$$\frac{\partial c}{\partial t} = D^*_{\text{eff}} \frac{\partial^2 c}{\partial y^2} . \tag{40}$$

---

[1] More exactly, this is a zone of the natural isotope composition which is considered as a background. Since the tracer concentration c is determined relative to this background [cf. Eq. (9)], this zone is referred to as « pure ^{16}O zone ».

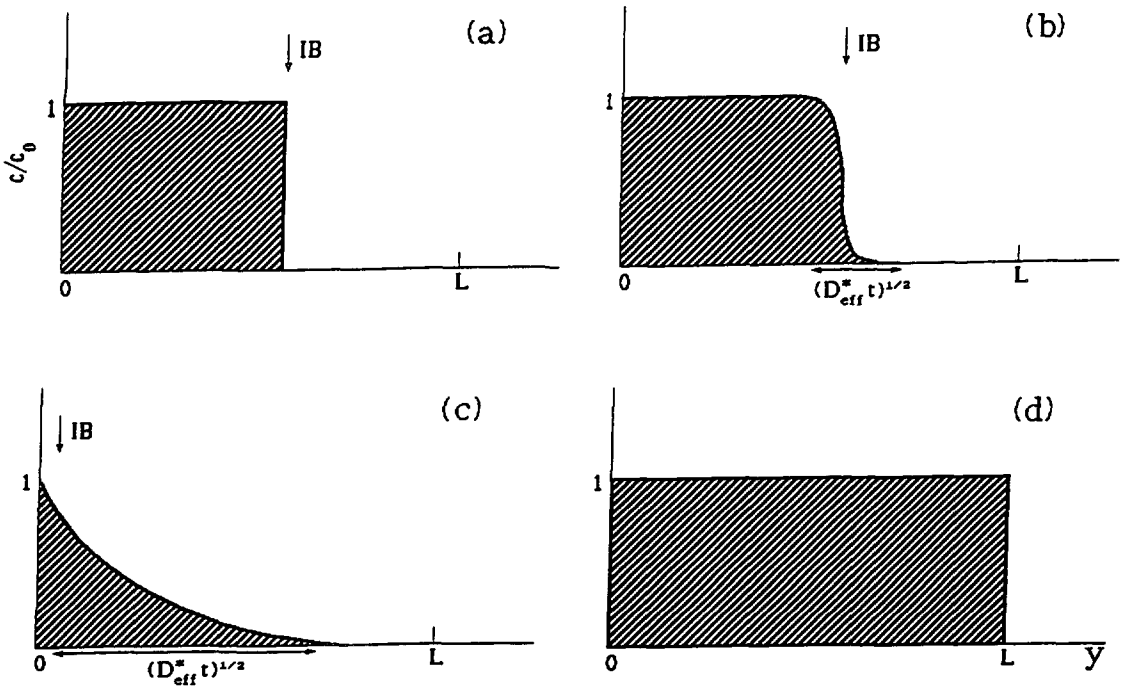

Fig. 2. — Schematic ^{18}O penetration profiles under the A-regime conditions. a) idealized and b) more realistic profile for the drift regime ; c) pure diffusion regime ; d) full isotope equilibrium.

Thus, there can be three essentially different situations, or kinetic regimes :

(i) *Diffusion regime,* when $y_{IB}(t) \ll (D^*_{eff}\, t)^{1/2} \ll L(t)$. This implies relatively short time t. Formally, the IB is located very close to the specimen surface. ^{18}O penetrates into the oxide film by means of ordinary self-diffusion, the penetration depth $(D^*_{eff}\, t)^{1/2}$ being much smaller than the total oxide thickness (Fig. 2c). The film growth has practically no effect on the tracer diffusion. These are the most convenient conditions for the tracer diffusion measurements. The tracer penetration profile is determined by the standard equation

$$c = c_0 \operatorname{erfc}\left[\frac{y}{2(D^*_{eff}\, t)^{1/2}}\right]. \tag{41}$$

Having measured the profile one can extract the effective self-diffusion coefficient of oxygen, D^*_{eff}.

(ii) *Drift regime,* when $(D^*_{eff}\, t)^{1/2} \ll y_{IB}(t) \ll L(t)$. This regime occurs after a longer annealing time t compared to that for the diffusion regime. We have a rather sharp IB which is located between the specimen surface and the oxide/metal interface and advances in depth according to equation (39). Note that the thickness of the pure ^{16}O zone remains $L(0) \simeq$ const.

(iii) *Full isotope equilibrium,* when we have $c \simeq c_0$ all over the oxide film (Fig. 2d).

The kinetic transition from the diffusion regime to the drift regime occurs at a moment t_1 at which $y_{IB}(t_1) = (D^*_{eff}\, t_1)^{1/2}$, where y_{IB} is determined by equation (39). In terms of the reduced variables

$$\tau = t/t_0 \quad \text{and} \quad \gamma = (2\,K/D^*_{eff})^{1/2}, \tag{42}$$

this relation takes the form

$$\gamma = \tau_1^{1/2}[(\tau_1 + 1)^{1/2} - 1]^{-1} \tag{43}$$

Consider in more detail the particular case when the second stage of the experiment is shorter than the first stage, i.e. $t \ll t_0$. Then equation (43) gives $\tau_1 \simeq 4/\gamma^2$, i.e.

$$t_1 \simeq 2\, D^*_{\text{eff}}\, t_0/K\,. \tag{44}$$

The lower diffusivity, the shorter is the duration of the diffusion regime and the sooner we come to the drift regime. Since $t \ll t_0$, equation (25) becomes $V_L \simeq (K/2\, t_0)^{1/2} = \text{const}$. Then, equation (34) can be solved analytically to give [15, 23]

$$c = \frac{c_0}{2}\left[\exp\left(\frac{V_L\, y}{D^*_{\text{eff}}}\right)\operatorname{erfc}\left(\frac{y + V_L\, t}{2(D^*_{\text{eff}}\, t)^{1/2}}\right) + \operatorname{erfc}\left(\frac{y - V_L\, t}{2\,(D^*_{\text{eff}}\, t)^{1/2}}\right)\right]. \tag{45}$$

This general solution describes penetration profiles for both the diffusion and the drift regimes. When $V_L\, t \ll (D^*_{\text{eff}}\, t)^{1/2}$, solution (45) reduces to (41) (diffusion regime), whereas for $V_L\, t \gg (D^*_{\text{eff}}\, t)^{1/2}$ this solution gives a step-like profile, shown in figure 2b, with an abrupt drop of the tracer concentration at $y_{IB} \simeq V_L\, t$ (drift regime). In the latter case one can measure y_{IB} and from this evaluate $V_L \simeq y_{IB}/t$ and then $K \simeq 2\, V_L^2\, t_0$. The moment t_1 of the diffusion/drift transition can be estimated from the condition $V_L\, t_1 = (D^*_{\text{eff}}\, t_1)^{1/2}$, from which it follows

$$t_1 = D^*_{\text{eff}}/V_L^2\,. \tag{46}$$

As it should be, with $V_L = (K/2\, t_0)^{1/2}$ this equation reduces to (44).

In most of « double-oxidation » experiments the second stage has been longer than the first one. Meanwhile, there seems to be an advantage in performing shorter-second-stage experiments. When the tracer penetration is relatively small ($\ell < L$) and the growth velocity remains nearly constant, the resultant tracer profiles can be properly interpreted in terms of simple analytical solutions like (37), (41) or (45). This advantage becomes even more pronounced when type C or especially type B regimes prevail (cf. Sect. 5 below and Part II of this work). In such cases deriving comprehensive analytical solutions is only possible under simplifying assumptions which can be met in shorter-second-stage experiments.

Even at $t \gg t_1$ the IB is diffuse to a thickness of about $(D^*_{\text{eff}}\, t)^{1/2}$ Therefore, due to continuous isotope exchange the pure ^{16}O zone is increasingly consumed until at $(D^*_{\text{eff}}\, t)^{1/2} \gg L(0)$ we arrive at full isotope equilibrium with $c \simeq c_0$ throughout the film (Fig. 2d). The moment t_2 of establishing full isotope equilibrium can be estimated from the condition $(D^*_{\text{eff}}\, t_2)^{1/2} = L(0) = (2\, Kt_0)^{1/2}$, which gives

$$t_2 = 2\, Kt_0/D^*_{\text{eff}}\,. \tag{47}$$

In terms of the reduced variables (42) this becomes

$$\tau_2 = \gamma^2 \tag{48}$$

Essentially, the above considered solution (45) holds at $t \ll t_2$ only.

The results of the above analysis are summarized as a kinetic diagram shown in figure 3. The lines of the diagram are determined by equations (43) and (48). Note that the diagram exhibits a critical point C at which $\tau_1(\gamma) = \tau_2(\gamma)$. This point has the coordinates

$$\gamma_C = 3^{1/2} \quad \text{and} \quad \tau_C = 3\,. \tag{49}$$

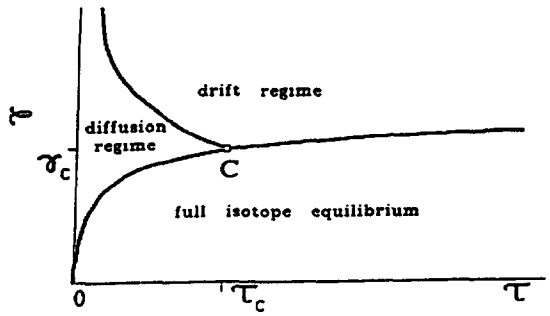

Fig. 3. — Kinetic diagram of oxygen tracer diffusion in a growing oxide film under the A-regime conditions. The reduced variables γ and τ are given by equations (42). The lines diffusion/drift and diffusion (drift)/equilibrium are determined by equations (43) and (48), respectively. Coordinates of the critical point C are determined by equations (49).

Above the critical point ($\gamma > \gamma_C$) the regimes change in time according to the sequence diffusion → drift → isotope equilibrium. This is the case for a relatively low diffusivity or/and a high velocity. Below the critical point ($\gamma < \gamma_C$) we can observe only the transition diffusion → isotope equilibrium, whereas the drift regime is no longer observed. This situation refers to a relatively high diffusivity or/and a low velocity. In either case, if the second stage is too long ($t > t_2$) nothing but nearly full isotope equilibrium can be observed. In contrast to this, from the profiles measured in the diffusion or drift regimes, which imply shorter-second-stage condition, one can determine the effective self-diffusion coefficient of oxygen D^*_{eff} or the parabolic rate constant K.

Note that the above analysis was based on the most general assumptions introduced in section 2. Therefore, no information about oxide growth or isotope diffusion mechanisms can be extracted from ^{18}O penetration profiles measured in type A conditions.

5. Analysis of penetration profiles in type C regime.

Now turn to another extreme, when a « double-oxidation » experiment is conducted at such a low temperature or/and for such a short second-stage time t that $(Dt)^{1/2} \ll \delta$. In this case, which is classified as C-regime [8, 9], the tracer penetrates into the GBs very much faster than into the bulk and the tracer leakage from the GBs, limited by bulk diffusion, can be neglected. Then, the tracer transport can be described by two independent equations :

$$\frac{\partial c'}{\partial t} = D' \frac{\partial^2 c'}{\partial y^2} - V' \frac{\partial c'}{\partial y}, \quad \text{(GB transport)} \tag{50}$$

$$\frac{\partial c}{\partial t} = D \frac{\partial^2 c}{\partial y^2} - V \frac{\partial c}{\partial y} \quad \text{(bulk transport)} \tag{51}$$

5.1 GRAIN BOUNDARIES IN ISOTOPE EQUILIBRIUM. — First of all, let us make sure that the present model is capable of quantitatively describing the concentration profile behaviour earlier predicted by Basu and Halloran [4] from simple mass balance arguments. Indeed, suppose that after getting in contact with the specimen the tracer very rapidly penetrates through the film, reaches the oxide/metal interface and immediately spreads over it. Therefore in the first approximation we can assume that from the very beginning we already have isotope equilibrium in the GBs and a constant tracer concentration c_0 both at the surface and at the

internal interface. Then, since bulk diffusion is nearly frozen out, the tracer penetrates from the interphase boundaries to the bulk by the mechanism of pure drift. In general, this results in the formation of two layers with bulk isotope equilibrium inside ($c \simeq c_0$) bounded by two sharp IBs (Fig. 4). The layer that is adjacent to the surface (the « outer » layer) grows with the velocity V which is determined by equation (15), i.e. $V = K_o/L$ where

$$K_o \equiv \frac{1}{kT} \int_{\mu_L}^{\mu_0} \left\{ D_O + \frac{n}{m} [\nu D'_M + (1 - \nu) D_M] \right\} d\mu . \tag{52}$$

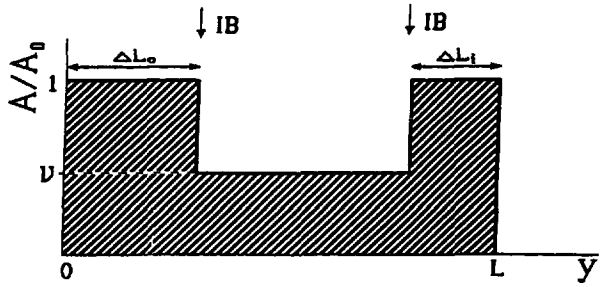

Fig. 4. — Schematic ^{18}O penetration profiles under the C-regime conditions. The GBs are in isotope equilibrium. The outer (ΔL_o) and the inner (ΔL_i) isotope layers label the new oxide layers growing at the surface and the oxide/metal interface, respectively.

An instantaneous thickness $\Delta L_o(t)$ of this isotope layer equals

$$\Delta L_o(t) = \int_0^t V \, dt = K_o \int_0^t L^{-1} \, dt . \tag{53}$$

Using the parabolic expression (24) for $L(t)$ one obtains

$$\Delta L_o(t) = (K_o/K) \, \Delta L(t) , \tag{54}$$

where $\Delta L(t)$ is the total thickness of the new oxide by a moment t (see Eq. (38)). The second IB obviously moves with the same velocity V, whereas the oxide/metal interface advances towards the metal with the total growth velocity $V_L = K/L$. Thus, the « inner » isotope layer bounded by the second IB and the oxide/metal interface increases in thickness with the velocity $V_L - V = (K - K_o)/L$. Repeating the above calculation, its thickness $\Delta L_i(t)$ also constitutes a constant fraction of $\Delta L(t)$, namely,

$$\Delta L_i(t) = (K_i/K) \, \Delta L(t) , \tag{55}$$

where

$$K_i = K - K_o = \frac{1}{kT} \int_{\mu_L}^{\mu_0} \nu (D'_O - D_O) \, d\mu . \tag{56}$$

Since $K_i + K_o = K$, the total thickness of the outer and the inner layers equals the total new oxide thickness : $\Delta L_o + \Delta L_i = \Delta L$. Furthermore, although during the film growth both of the isotope layers also grow, their ratio

$$\Delta L_o(t)/\Delta L_i(t) = K_o/K_i$$

remains constant and depends only on interrelation among the diffusivities involved in the problem. Note also that the thickness of the pure ^{16}O layer between the two IBs remains $L(0) = const.$

According to Basu and Halloran [4], the outer and the inner isotope layers are nothing but new oxide layers growing at the surface and at the oxide/metal interface due to metal outward and oxygen inward diffusion, respectively. In the present model the corresponding oxide growth velocities are given by equations (5) and (6), from which one has $V_1 = K_1/L$ and $V_2 = K_2/L$ with

$$K_1 = \frac{1}{kT} \int_{\mu_L}^{\mu_0} \frac{n}{m} [\nu D'_M + (1 - \nu) D_M] \, d\mu \,, \tag{57}$$

$$K_2 = \frac{1}{kT} \int_{\mu_L}^{\mu_0} [\nu D'_O + (1 - \nu) D_O] \, d\mu \,. \tag{58}$$

The tracer ideally labels the new oxide, as it was suggested in [4], if

$$K_o = K_1 \quad \text{and} \quad K_i = K_2 \,. \tag{59}$$

Comparing equations (57) and (58) with (52) and (56) one can notice that

$$K_o - K_1 = K_2 - K_i = \frac{1}{kT} \int_{\mu_L}^{\mu_0} D_O \, d\mu \,. \tag{60}$$

This relation shows that Basu and Halloran's conclusions are valid when the contribution from the oxygen bulk transport, represented by the right-hand side of equation (60), is vanishing. This means that at any depth $D_O \ll \nu D'_O$, i.e. the oxide growth is controlled either by GB diffusion of oxygen or by metal diffusion, or by their combination. Formally, if the oxide growth is limited by oxygen bulk diffusion ($D_O \gg \nu D'_O$) relations (59) no longer hold. But in this case in the C-regime conditions both the isotope and the new oxide layers have atomic sizes and can hardly be reliably measured in experiments.

5.2 GRAIN BOUNDARIES FAR FROM ISOTOPE EQUILIBRIUM. — It should be reminded that the above considered features of the tracer profile behaviour relate to later stages of the tracer transport when we already have isotope equilibrium in the GBs. It seems interesting, however, to study earlier stages of the process when the profiles show GB-related tails, analysis of which makes it possible to evaluate the transport properties of the GBs in the oxide.

Before the tracer has reached the oxide/metal interface we can observe at most the outer isotope layer and therefore only one IB moving with the velocity V. To simplify the further analysis, let us come over for a while to the reference system fixed to this IB. Formally this means that we introduce a new coordinate $Y = y - \Delta L_o(t)$ instead of y. Then, equations (50) and (51) take the form

$$\frac{\partial c'}{\partial t} = D' \frac{\partial^2 c'}{\partial Y^2} - \tilde{V}' \frac{\partial c'}{\partial Y} \quad \text{(GB transport)} \tag{61a}$$

$$\frac{\partial c}{\partial t} = D \frac{\partial^2 c}{\partial Y^2} \quad \text{(bulk transport)} \,. \tag{61b}$$

Now we have pure diffusion in the bulk, which is negligible, and driven diffusion along the GBs with the boundary condition $c = c_0$ at $Y = 0$. In the new system of reference the

oxide/metal interface moves with the velocity

$$\tilde{V}_L = V_L - V = K_i/L\,, \tag{62}$$

whereas the GB drift velocity becomes

$$\tilde{V}' = V' - V = K_i/\nu L\,. \tag{63}$$

(We have used Eqs. (15), (16) and (26)).

The resultant kinetic behaviour in the GBs is more or less similar to the tracer penetration into an oxide film under the A-regime conditions (see Sect. 4). At the very beginning we are in the pure diffusion regime and the tracer penetration along the GBs results in an erfc-shaped tail (Fig. 5a)

$$A = c_0\,\nu\,\mathrm{erfc}\left[\frac{y - \Delta L_0(t)}{2(D' t)^{1/2}}\right]. \tag{64}$$

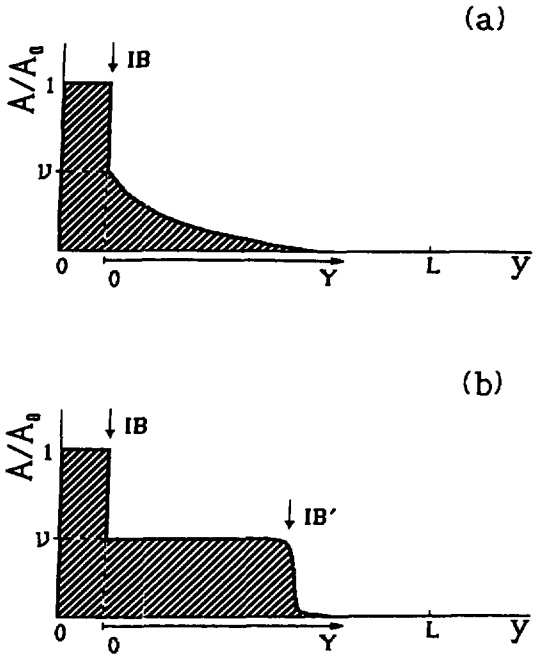

Fig. 5. — Schematic ^{18}O penetration profiles under the C-regime conditions. The GBs are far from isotope equilibrium. The GB penetration proceeds in the diffusion regime a) or the drift regime b).

Having measured the profile, one can determine the GB self-diffusion coefficient of ^{18}O, D'. If metal outward diffusion is negligible, the outer isotope layer is missing and the GB-related tail starts immediately at the surface. Notably, in that case the measured tracer concentration near the surface, $A \simeq c_0\,\nu$, will be considerably lower than the tracer content c_0 in the atmosphere. In principle, this difference allows one to estimate the grain size d assuming a reasonable value for δ.

At a certain moment t_1' a diffusion/drift transition in the GBs should occur and at $t \gg t_1'$ the tracer penetration along the GBs proceeds in the drift regime. Then we have a sharp isotope boundary in the GBs, IB', moving with the velocity $\tilde{V}'$ (Fig. 5b). Its instantaneous location is determined by

$$Y_{\mathrm{IB}'}(t) = \int_0^t \tilde{V}'\, dt = \frac{2K_1}{\nu(2K)^{1/2}} \left[(t + t_0)^{1/2} - t_0^{1/2}\right]. \tag{65}$$

The moment t_1' of the diffusion/drift transition in the GBs can be estimated from the condition $(D' t_1')^{1/2} = Y_{\mathrm{IB}'}(t_1')$. In terms of the reduced variables

$$\tau = \frac{t}{t_0} \quad \text{and} \quad \gamma' = \frac{2K_i}{\nu(2KD')^{1/2}} \tag{66}$$

this condition has the form

$$\gamma' = (\tau_1')^{1/2} \left[(\tau_1' + 1)^{1/2} - 1\right]^{-1} \tag{67}$$

The GB diffusion/drift transition can be observed in shorter-second-stage experiments. The drift velocity $\tilde{V}' \simeq K_i/\nu(2Kt_0)^{1/2}$ is then constant and the transition time equals $t_1' \simeq 2\nu^2(K/K_i^2) D' t_0$. By analogy to equation (45), the general solution describing the tracer concentration profiles both in the diffusion and the drift regimes has the form

$$A = \nu \frac{c_0}{2} \left[\exp\left(\frac{\tilde{V}' Y}{D'}\right) \operatorname{erfc}\left(\frac{Y + \tilde{V}' t}{2(D' t)^{1/2}}\right) + \operatorname{erfc}\left(\frac{Y - \tilde{V}' t}{2(D' t)^{1/2}}\right)\right]. \tag{68}$$

Sooner or later a moment t_2' comes when the tracer reaches the oxide/metal interface and at $t \gg t_2'$ we have isotope equilibrium in the GBs. There can be two ways to come to this isotope equilibrium : either from the drift regime or from the diffusion regime. In the first case the moment t_2' can be found from the condition $Y_{\mathrm{IB}'}(t_2') = L(0)$. Indeed, equations (62) and (63) show that the oxide/metal interface moves by a factor of $\nu(\ll 1)$ more slowly than the IB'. Therefore, while estimating the moment t_2' when the IB' reaches the interface the latter can be considered as motionless. In the same approximation, the condition for the GB diffusion/equilibrium transition can be taken in the form $(D' t_2')^{1/2} = L(0)$. To allow for both of the above possibilities, the condition of coming to the GB isotope equilibrium can be formulated as $Y_{\mathrm{IB}'}(t_2') + (D' t_2')^{1/2} = L(0)$. In terms of the reduced variables (66) this condition takes the form

$$\gamma' = (\tau_2')^{1/2} \left[1 + q - (\tau_2' + 1)^{1/2}\right]^{-1}, \tag{69}$$

where the constant coefficient q is determined by $q = \nu K/K_i$. When $\gamma' \ll 1$, equation (69) reduces to

$$\gamma' \simeq (\tau_2')^{1/2}/q, \tag{70}$$

which equation is similar to equation (48) for the A-regime. However, as γ' increases τ_2' tends to a finite value

$$\tau^* = q^2 + 2q. \tag{71}$$

To compare, in the case of the A-regime τ_2 unlimitedly increases with γ (cf. Fig. 3). The latter is understandable since in the A-regime the IB and the oxide/metal interface move with equal

velocities and full isotope equilibrium is therefore attained by means of diffusion controlled isotope exchange between the pure ^{16}O zone ($y > y_{IB}$) and the zone of isotope equilibrium ($y < y_{IB}$). The lower the diffusivity, the longer is the time to reach the equilibrium. By contrast, in the case of the C-regime the IB′ moves much faster than the oxide/metal interface and due to this can always reach it in a *finite* time (71) regardless of the GB diffusivity D'.

Figure 6 represents the above discussed conditions for possible kinetic regimes in the form of a kinetic diagram. The boundaries between the areas corresponding to various regimes are determined by equations (67) and (69). The critical point C has the coordinates

$$\tau'_C = q + q^2/4 \quad \text{and} \quad \gamma'_C = (1 + 4/q)^{1/2} \tag{72}$$

Independent of γ' the tracer penetration into the GBs starts in the diffusion regime. Below the critical point ($\gamma' < \gamma'_C$) we come to the GB isotope equilibrium directly from the diffusion regime, while above the critical point ($\gamma' > \gamma'_C$) we first come to the GB drift regime and afterwards arrive at the GB isotope equilibrium. In either case, the time to attain the GB isotope equilibrium is never larger than the value τ^* given by equation (71).

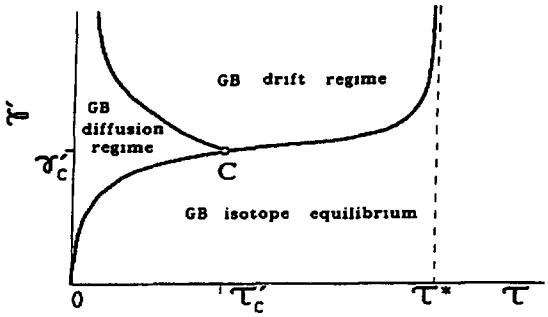

Fig. 6. — Kinetic diagram of oxygen tracer penetration along the GBs in a growing oxide film under the C-regime conditions. The reduced variables γ' and τ are given by equations (66). The lines diffusion/drift and diffusion (drift)/equilibrium are determined by equations (67) and (69), respectively. Coordinates of the critical point C are determined by equation (72). The upper limit of time-to-equilibrium, τ^*, is given by equation (71).

Let us consider two specific cases. First, suppose that the oxide film growth is controlled by oxygen inward GB-diffusion. For this case equations (52) and (56) yield $K_i \simeq K$ and $K_o \to 0$ (no outer isotope layer). Then we have $\gamma' = \frac{1}{\nu}(2K/D')^{1/2}$, $q \simeq \nu$, $\tau'_C \simeq \nu$ and $\gamma'_C \simeq 2/\nu^{1/2}$. According to equation (71), the time to the GB isotope equilibrium is not larger than $2\,\nu t_0$. Since $\nu \ll 1$, the equilibrium is attained very shortly compared with the first-stage duration t_0 and immediately after that the inner isotope layer, as was discussed previously, should appear. If the initial film thickness $L(0)$ is sufficiently large, the isotope penetration profiles during this relatively short period can in principle be measured. It is not clear *a priori* whether the pure GB diffusion regime will be observed in this case or not. If oxygen transport is dominated by the interstitial mechanism, the rate constant equals [20] $K \simeq \nu(1 + z)D'_O$, where z is the charge of oxygen ions, D'_O the GB self-diffusivity of oxygen near the surface. From this estimation the actual value of γ' is $[2(1 + z)/f'\,\nu]^{1/2}$. This value is only slightly above γ'_C and therefore both the diffusion and drift regimes can in principle be observed. In the case of a vacancy mechanism of oxygen transport, the above equation for K is again

applicable, but now with the oxygen diffusivity near the oxide/metal interface, which is considerably higher than that near the surface. Consequently, the value of γ' is larger than that for the interstitial mechanism and the duration of the GB diffusion regime is shorter (cf. Fig. 6). In that case it is most probable that the measured GB-related tail of the tracer profile will exhibit a step-like shape as it is sketched in figure 5b. The step's coordinate $Y_{IB'}$ allows one to evaluate the GB drift velocity $\tilde{V}' = Y_{IB'}/t$ and then K or ν using the relation $\tilde{V}' = (K/2\,t_0)^{1/2}/\nu$.

In the other extreme, the oxide growth is strongly controlled by metal outward diffusion and therefore we have $K_0 \simeq K$ while $K_i \to 0$. Then both $\tilde{V}'$ and $\tilde{V}_L$ are very small and the tracer transport reduces to nearly pure diffusion along the GBs in a finite-thickness layer $0 \leqslant Y \leqslant L(0)$. Since $q = \nu K/K_i \gg 1$, the value of γ' is much smaller than $\gamma'_C \simeq 1$ and the GB drift regime is not realized. The time to the GB isotope equilibrium can be estimated from equation (70) to give $t'_2 \simeq (2\,K/D')\,t_0 \gg t_0$. Unless the first stage of the experiment is too short compared with the second one, the condition $t < t'_2$ holds and a relatively deep outer isotope layer can be expected to form, followed by an erfc-type GB-related tail (see Fig. 5a) from which the GB-diffusion coefficient D' can be extracted.

Finally, note that in reality the equilibrium isotope concentration c_0 arises at the oxide/metal interface not instantaneously but gradually during a finite period of time δt. Consequently, the second IB in figure 4 should be smeared to a layer of thickness $\delta L \simeq \tilde{V}_L\,\delta t$. When $\gamma' > \gamma'_C$ and we come to the GB isotope equilibrium from the drift regime, δt can be estimated as $\delta t \simeq (D'\,t'_2)^{1/2}/\tilde{V}'$. Then $\delta L \simeq (\tilde{V}_L/\tilde{V}')\,(D'\,t'_2)^{1/2} \ll \nu L(0)$ (cf. Eqs. (62) and (63)), i.e. the thickness of the second IB is relatively small. If $\gamma' < \gamma'_C$ and we arrive at the GB isotope equilibrium from the diffusion regime, $\delta t \simeq L^2/D'$ and therefore $\delta L \simeq (K_i/D')\,L$. Then the situation depends on the oxygen transport mechanism. In case of the interstitial mechanism $K_i \propto \nu D'$ and $\delta L \simeq \nu L$, i.e. the IB is again relatively sharp. Under the vacancy mechanism K_i can be much larger than $\nu D'$ and the ratio $\delta L/L$ is not small. The second IB is then rather diffuse (Fig. 7). Notably, this spreading of the IB is entirely accounted for by GB diffusion and has nothing in common with bulk diffusion or with the GB/bulk isotope exchange.

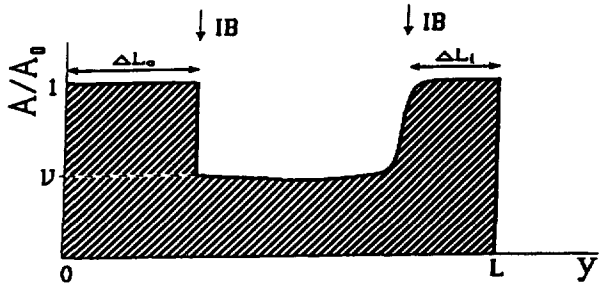

Fig. 7. — The same profile as in figure 4 but the second isotope boundary is smeared due to GB diffusion.

6. Discussion and conclusions.

Thus, we have proposed a model for oxygen tracer diffusion in a growing oxide film in the course of a two-stage oxidation experiment. The model is based on a number of simplifying assumptions, some of which are unfortunately far from the real picture of oxide growth. We

have assumed that the electronic transport number $t_e = 1$ while in reality t_e can be sometimes appreciably less than unity depending on the doping level. Also, growing oxide films usually exhibit a much more complicated structure than it is adopted in the parallel GBs model. For instance, a variation of the grain size across a film may strongly influence the resultant oxygen tracer profiles [24]. Furthermore, such factors as stresses generation, the formation of cavities and protrusions at the oxide/metal interface or whiskers at the surface may obviously have an even more drastic effect on the ^{18}O profiles shape [3]. All these and other important factors remain beyond the scope of the present model.

Moreover, even if macrostructure of a film perfectly complies with the geometry assumed in this model the diffusivities of the species may significantly change across the growing film, sometimes by orders of magnitude. This variation of the diffusivities is unavoidable (unless the film is too thick and its growth rate is negligible) and arises from the peculiarities of the atomic mechanisms of chemical diffusion in ionic crystals. Specifically, oxygen inward transport can be provided by an excess oxygen interstitials generation at the surface and their diffusion towards the oxide/metal interface. As a result, the oxygen self-diffusion coefficient near the surface can be much higher than that close to the oxide/metal interface. In case of the vacancy mechanism oxygen vacancies are consumed near the surface and the resultant vacancy concentration gradient causes a vacancy flux from the oxide/metal interface towards the surface thereby giving rise to an opposite flux of oxygen. Again, the variation of the defect concentration results in a variation of the oxygen self-diffusion coefficient across the film. Therefore, the use of constant diffusivities of oxygen, D and D', is a very strong assumption of the model. This and other oversimplifying assumptions should be accepted as a first approximation that will probably be reconsidered in the future.

Even in this simplified formulation the model describes a large variety of possible oxygen tracer profiles depending on interrelation among the key parameters of the model. These parameters, in turn, depend on the oxygen and metal self-diffusion coefficients along the GBs and in the bulk as well as on the geometrical factors and durations of the first and the second stages of the « double-oxidation » experiment. Partly, this variety is due to the fact that the present model is more general than the spherical grain model [4, 5]. The latter is applied only when oxygen GB diffusion is the dominating mechanism of the oxide growth, while the parallel GBs model is independent of the growth mechanism. This makes this model potentially applicable to a larger amount of oxides or other solid-gas reaction products.

In its exact formulation (Eqs. (31), (32), (18)-(23)), the model is intended for computer simulations of oxygen tacer profiles. However, in this paper we have considered some specific cases when the model equations can be solved analytically or at least tracer profiles behaviour can be easily predicted from the basic equations. In the A-regime, which can be realized at higher temperatures or in fine-grained oxides, the oxide film behaves as a virtually homogeneous medium with the effective oxygen diffusion coefficient (35). The other extreme is represented by the C-regime which implies a relatively low temperature or/and a short annealing time. In this case ^{18}O profiles are determined by the tracer diffusion along the GBs and ^{18}O incorporation in new oxide layers. In full agreement with the mass balance analysis [4] the model-based profiles depend on the prevailing mechanism of the oxide growth.

In both A and C type regimes the tracer penetration exhibits similar features. In both cases one can distinguish three kinetic regimes : the pure diffusion regime, the drift regime, and the regime of full isotope equilibrium. Then, possible experimental situations can be conveniently described by the kinetic diagrams shown in figures 3 and 6. The reduced variables γ' and γ represent interrelation between the rate of oxygen tracer diffusion along the GBs (γ') or in the bulk (γ) and the rate of oxide growth which determines the driving force acting on the oxygen tracer. The sequence and duration of the kinetic regimes essentially depend on whether $\gamma' > \gamma'_C(\gamma > \gamma_C)$ or $\gamma' < \gamma'_C(\gamma < \gamma_C)$. The first case corresponds to strongly driven

diffusion whereas in the second case we have nearly pure diffusion without drift. The diagrams in figures 3 and 6 can be useful in designing « double-oxidation » experiments. They show, in particular, that valuable information about oxygen GB self-diffusion and oxide growth mechanisms can be obtained in shorter-second-stage experiments where the tracer penetration depth into the film is smaller than the film thickness.

In part II of this work we shall study a type B regime of tracer diffusion when $\delta < (Dt)^{1/2} < d/2$. Mathematically, this case is much more complicated than the A and C-regimes considered in this paper. However, the problem is more or less analogous to the problem of GB-electromigration [11, 13-16] or diffusion along moving GBs [25]. Applying the same mathematical techniques, we shall present analytical solutions and propose methods of tracer profile treatment for GB self-diffusion parameter determination. Thereby the analysis of all specific cases of the proposed model will have been complete.

Acknowledgements.

Fruitful discussions with Dr. J. Jedlinski and Dr. W. Wegener are gratefully acknowledged. This work was supported by the Deutsche Forschungsgemeinschaft.

References

[1] ATKINSON A., Diffusion Phenomena in Thin Films and Microelectronic Materials, D. Gupta and P. S. Ho Eds. (Park Ridge, NJ, 1988) p. 204.
[2] PHILIBERT J., *Defect Diffusion Forum* **59** (1988) 63.
[3] JEDLINSKI J., *Solid State Phenomena* **21** & **22** (1992) 335.
[4] BASU N. S. and HALLORAN J. W., *Oxid. Met.* **27** (1987) 143.
[5] WEGENER W. and BORCHARDT G., *Oxid. Met.* **36** (1991) 339.
[6] OISHI Y. and ICHIMURA H., *J. Chem. Phys.* **71** (1979) 2281.
[7] BOKSHTEIN B. S., MAGIDSON I. A. and SVETLOV I. L., *Phys. Met. Metall.* **6** (1958) 81.
[8] HARRISON L. G., *Trans. Faraday Soc.* **57** (1961) 1191.
[9] KAUR I. and GUST W., Fundamentals of Grain and Interphase Boundary Diffusion (Ziegler Press, Stuttgart, 1988).
[10] HART E. W., *Acta Metall.* **5** (1957) 597.
[11] GUPTA D., CAMPBELL D. R. and HO P. S., Thin Films : Interdiffusion and Reactions J. M. Poate, K. N. Tu and J. W. Mayer Eds. (Wiley, NY, 1978) p. 161.
[12] MISHIN Yu. M. and RAZUMOVSKII I. M., *Acta Metall. Mater.* **40** (1992) 597.
[13] MARTIN G., *Phys. Stat. Solidi A* **14** (1972) 183.
[14] TAI K. L., SUN P. H. and OHRING M., *Thin Solid Films* **25** (1975) 343.
[15] TAI K. L. and OHRING M., *J. Appl. Phys.* **48** (1977) 28.
[16] TAI K. L. and OHRING M., *J. Appl. Phys.* **48** (1977) 36.
[17] ATKINSON A., TAYLOR R. I. and GROODE P. D., *Oxid. Met.* **13** (1979) 519.
[18] SHEASBY J. S. and BROWN J. D., *Oxid. Met.* **5** (1978) 405.
[19] ATKINSON A. and TAYLOR R. I., *High Temperatures-High Pressures* **14** (1982) 571.
[20] KOFSTAD P., High Temperature Corrosion (Elsevier Applied Science, London, NY, 1988).
[21] FISHER J. C., *J. Appl. Phys.* **22** (1951) 74.
[22] WHIPPLE R. T. P., *Philos. Mag.* **45** (1954) 1225.
[23] BOLTAKS B. I., Diffusion in Semiconductors (Academic Press, NY, 1963) p. 117.
[24] QUADAKKERS W. J., ELSCHNER A., SPEIER W. and NICKEL H., *Appl. Surf. Sci.* **52** (1991) 271.
[25] MISHIN Yu. M. and RAZUMOVSKII I. M., *Acta Metall. Mater.* **40** (1992) 839.